SUPPLEMENTAL FIGURE LEGENDS

Figure S1. Related to Figure 1

(A) STRING database co-occurance analysis based on the proteins used in the network in Figure 1B. Each square and the associated colour indicates the presence or absence and degree of conservation.

(B) Treefam data showing percent species with Aquarius/EMB-4 in each clade.

(C) Treefam tree based on sequence conservation of Aquarius/EMB-4 proteins in different model organisms (bootstrap values are indicated on branches).

(D) Assembly of splicing factors, Aquarius/EMB-4 and exon junction complex proteins during different stages of RNA splicing. Aquarius assembles during the B complex formation on intronic RNA and stays for the rest of the splicing reactions. EJC proteins assemble during Bact complex formation.

(E) Validation of the anti-EMB-4 antibody used in this study. The monoclonal anti-EMB-4 antibody (5M19-8) detects a single band at the size corresponding to EMB-4 (170kD) in wild type animals and no band is detected in the null *emb-4(hc60)* mutants (alpha-tubulin is used as loading control).

(F) Immunoprecipitation of EMB-4 using anti-EMB-4 antibodies and western blotting for EMB-4 and FLAG::HRDE-1.

Figure S2. Related to Figure 2

Immune-staining of *C. elegans* germline with anti-EMB-4 antibodies. Each panel highlights a different part of the germline.

Figure S3. Related to Figure 3

(A) *mjIs144* transgene consists of *mex-5* promoter, GFP sequence with 3 synthetic introns, histone H2B sequence for nuclear localisation, piRNA target site for 21UR-1, *tbb-2* UTR and is inserted in Chr II by MosSCI single copy insertion. *mjIs144* transgene is fully silenced in wild type animals and de-silences in *hrde-1* and *emb-4* mutants.

(B) *ccSi1504* transgene consists of *smu-1* promoter, SV40 nuclear localisation signal, GFP sequence where all piRNA target sequences are removed (Frøkjær-Jensen et al. 2016), 4 *smu-1* introns, EGL-13 nuclear localisation signal, piRNA target site for 21UR-1, *smu-1* 3`UTR and is inserted in Chr V by MosSCI single copy insertion. *ccSi1504* is fully silenced in wild type animals and de-silences in *hrde-1* and *emb-4* mutants (numbers show individual

animals assayed).

Figure S4. Related to Figure 4

(A) Domain structure of EMB-4 based on the domain structure of Aquarius (De et al. 2015).

(B) Crystal structure of Aquarius (domains are highlighted with same colours as in Figure S4A.

(C) Structural alignment of Aquarius (white) and EMB-4 (red).

(D) Superimposition of Vasa/AMPPNP/ssRNA with the crystal structures of Aquarius, EMB-4 and yeast Upf1-RNA. G884 residue of EMB-4 (shown in red) is embedded in close proximity to the putative ssRNA binding pocket.

(E) Western-blot showing EMB-4 protein abundance in wild type and *emb-4(sa44)* adult stage animals.

Figure S5. Related to Figure 5.

Enrichment of genes in 22G-RNA density bins used in Figure 5H-I for germline and somatic 22G-RNA targets (Gu et al. 2009), for WAGO class 22G-RNA targets (Gu et al. 2009), for piRNA target genes (top 500, (Bagijn et al. 2012), for ERGO-1 target genes (Conine et al. 2010; Han et al. 2009), for ALG-3/4 target genes (Conine et al. 2010; Han et al. 2009) and for CSR-1 target genes (Claycomb et al. 2009).

Figure S6. Related to Figure 6.

mRNA and 22G-RNA profiles of (A) piRNA target gene *bath-45*, (B) CER-15 retro-element, and (C) Mirage1 transposable element

Figure S7. Related to Figure 7.

22G-RNA profiles of wild-type, *hrde-1* and *emb-4* mutant animals (mean 22G-RNA abundance of three replicates) on (A) three intron piRNA sensor and (B) single intron piRNA sensor (Y-axis scale in wild type animals and mutants are different).

Figure S8. Related to Figure 7.

(A, B) mRNA expression levels correlate negatively with 22G-RNA abundance and correlation increases when more exons are targeted by 22G-RNAs (black line vs red line).

References

Bagijn, Marloes P., Leonard D. Goldstein, Alexandra Sapetschnig, Eva-Maria Weick, Samir Bouasker, Nicolas J. Lehrbach, Martin J. Simard, and Eric A. Miska. 2012. “Function, Targets, and Evolution of Caenorhabditis Elegans piRNAs.” *Science* 337 (6094). AAAS: 574–78.

Claycomb, Julie M., Pedro J. Batista, Ka Ming Pang, Weifeng Gu, Jessica J. Vasale, Josien C. van Wolfswinkel, Daniel A. Chaves, et al. 2009. “The Argonaute CSR-1 and Its 22G-RNA Cofactors Are Required for Holocentric Chromosome Segregation.” *Cell* 139 (1). Elsevier: 123–34.

Conine, Colin C., Pedro J. Batista, Weifeng Gu, Julie M. Claycomb, Daniel A. Chaves, Masaki Shirayama, and Craig C. Mello. 2010. “Argonautes ALG-3 and ALG-4 Are Required for Spermatogenesis-Specific 26G-RNAs and Thermotolerant Sperm in Caenorhabditis Elegans.” *Proceedings of the National Academy of Sciences of the United States of America* 107 (8). National Acad Sciences: 3588–93.

De, Inessa, Sergey Bessonov, Romina Hofele, Karine dos Santos, Cindy L. Will, Henning Urlaub, Reinhard Lührmann, and Vladimir Pena. 2015. “The RNA Helicase Aquarius Exhibits Structural Adaptations Mediating Its Recruitment to Spliceosomes.” *Nature Structural & Molecular Biology* 22 (2). Nature Publishing Group: 138–44.

Frøkjær-Jensen, Christian, Nimit Jain, Loren Hansen, M. Wayne Davis, Yongbin Li, Di Zhao, Karine Rebora, et al. 2016. “An Abundant Class of Non-Coding DNA Can Prevent Stochastic Gene Silencing in the C. Elegans Germline.” *Cell* 166 (2): 343–57.

Gu, Weifeng, Masaki Shirayama, Darryl Conte Jr., Jessica Vasale, Pedro J. Batista, Julie M. Claycomb, James J. Moresco, et al. 2009. “Distinct Argonaute-Mediated 22G-RNA Pathways Direct Genome Surveillance in the C. Elegans Germline.” *Molecular Cell* 36 (2). Elsevier Inc.: 231–44.

Han, Ting, Arun Prasad Manoharan, Tim T. Harkins, Pascal Bouffard, Colin Fitzpatrick, Diana S. Chu, Danielle Thierry-Mieg, Jean Thierry-Mieg, and John K. Kim. 2009. “26G Endo-siRNAs Regulate Spermatogenic and Zygotic Gene Expression in Caenorhabditis Elegans.” *Proceedings of the National Academy of Sciences of the United States of America* 106 (44). National Acad Sciences: 18674–79.

Figure S1

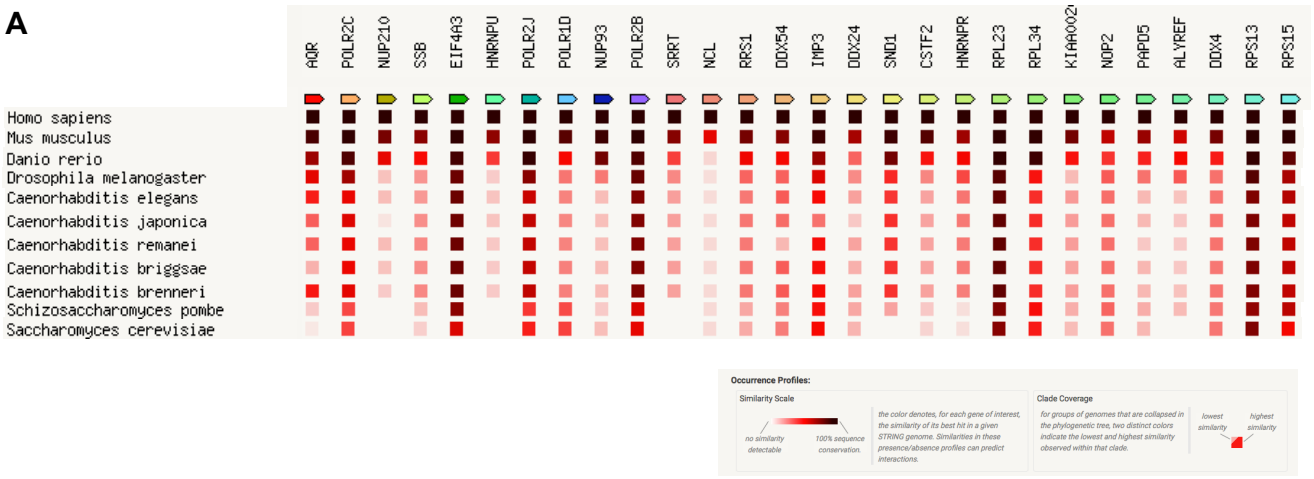
A
AQR
POLR2C
NUP210
SSB
EIF4A3
HNRNPU
POLR2J
POLR1D
NUP93
POLR2B
SRRT
NCL
RRS1
DDX54
IMP3
DDX24
SND1
CSTF2
HNRNPR
RPL23
RPL34
KIAA0020
NOP2
PAPD5
ALYREF
DDX4
RPS13
RPS15
Homo sapiens
Mus musculus
Danio rerio
Drosophila melanogaster
Caenorhabditis elegans
Caenorhabditis japonica
Caenorhabditis remanei
Caenorhabditis briggsae
Caenorhabditis brenneri
Schizosaccharomyces pombe
Saccharomyces cerevisiae
Occurrence Profiles:
Similarity Scale
Clade Coverage

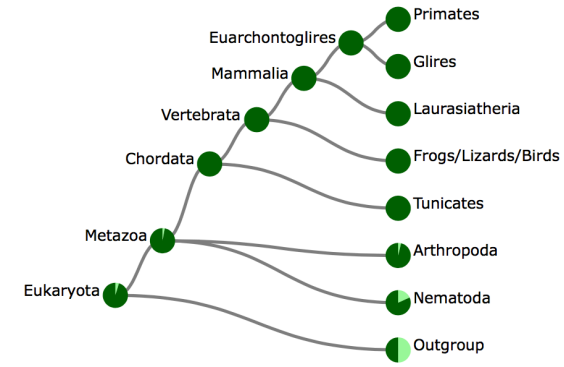
B
Primates
Glires
Laurasiatheria
Frogs/Lizards/Birds
Tunicates
Arthropoda
Nematoda
Outgroup
Euarchontoglires
Mammalia
Vertebrata
Chordata
Metazoa
Eukaryota

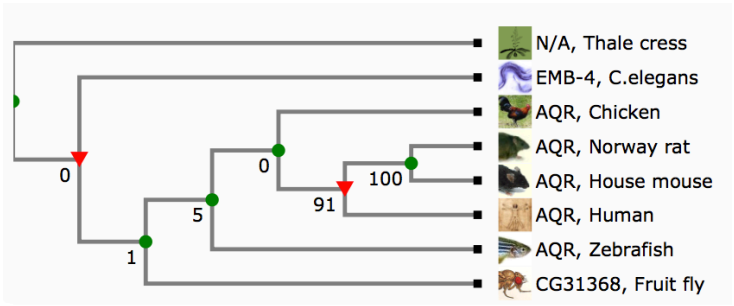
C
N/A, Thale cress
EMB-4, C.elegans
AQR, Chicken
AQR, Norway rat
AQR, House mouse
AQR, Human
AQR, Zebrafish
CG31368, Fruit fly
0
0
100
91
5
1

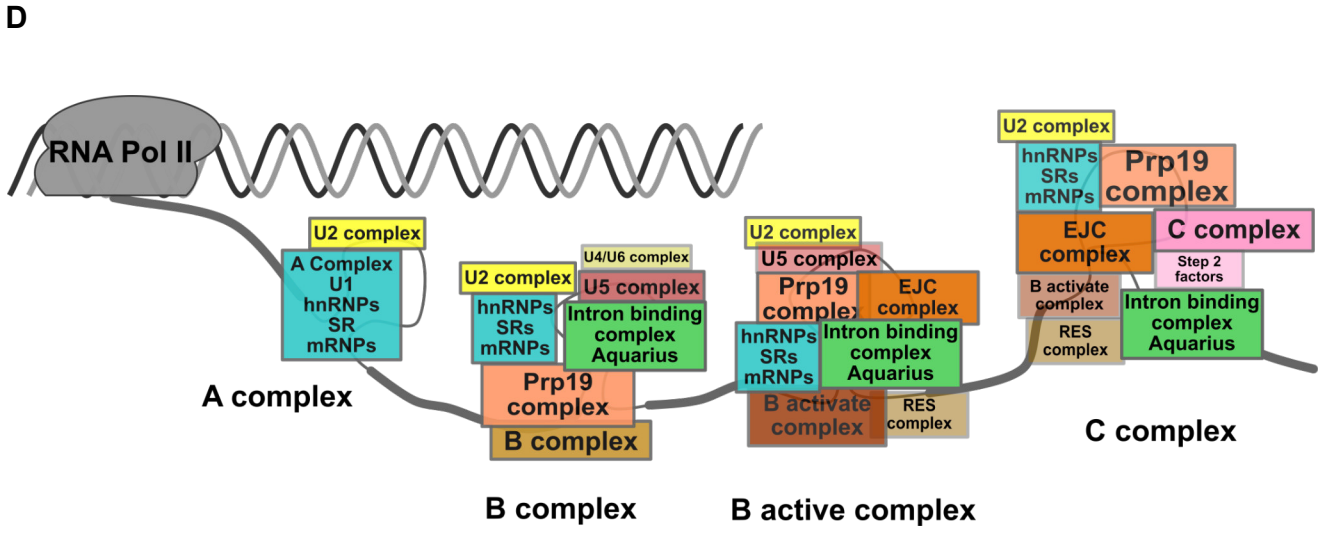
D
RNA Pol II
U2 complex
A Complex
U1
hnRNPs
SR
mRNPs
A complex
U2 complex
U4/U6 complex
U5 complex
hnRNPs
SRs
mRNPs
Intron binding
complex
Aquarius
Prp19
complex
B complex
B complex
U2 complex
U5 complex
Prp19
EJC
complex
hnRNPs
SRs
mRNPs
Intron binding
complex
Aquarius
B activate
complex
RES
complex
B active complex
U2 complex
hnRNPs
SRs
mRNPs
Prp19
complex
EJC
complex
C complex
Step 2
factors
B activate
complex
Intron binding
complex
Aquarius
RES
complex
C complex

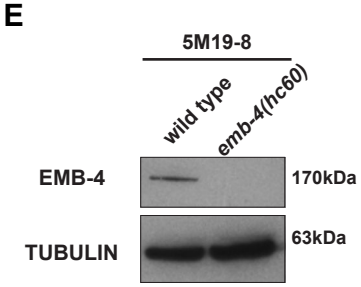
E
5M19-8
wild type
emb-4(hc60)
EMB-4
170kDa
TUBULIN
63kDa

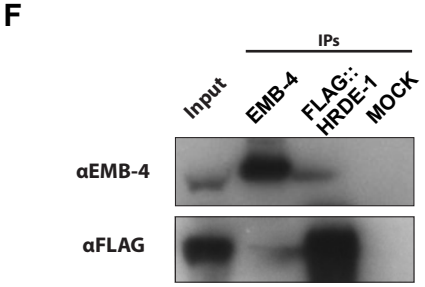
F
IPs
Input
EMB-4
FLAG::
HRDE-1
MOCK
αEMB-4
αFLAG

Figure S2

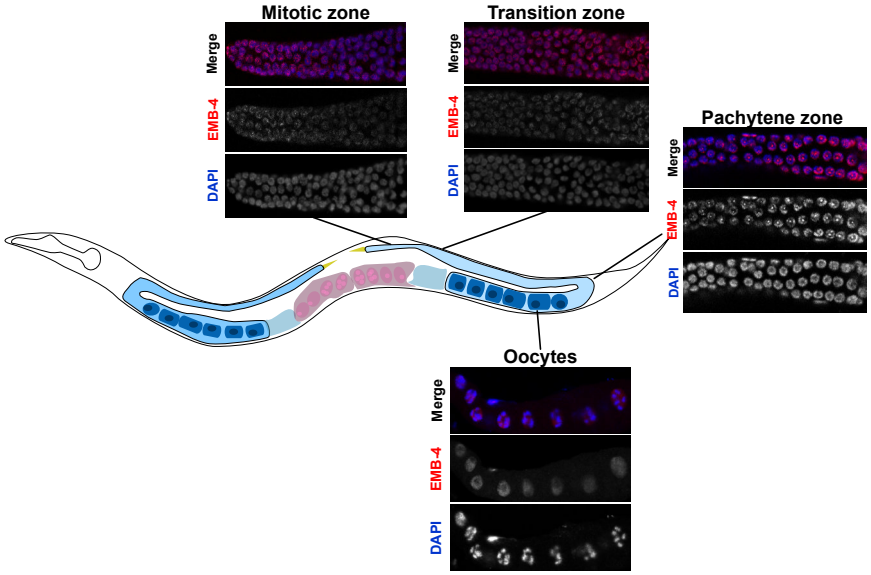
Mitotic zone
Merge
EMB-4
DAPI
Transition zone
Merge
EMB-4
DAPI
Pachytene zone
Merge
EMB-4
DAPI
Oocytes
Merge
EMB-4
DAPI

Figure S3

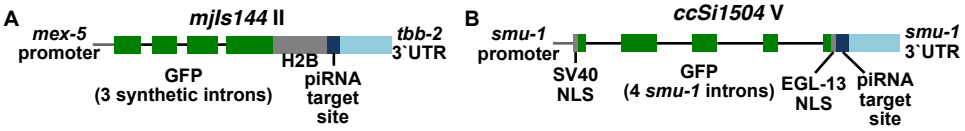

Wild type	*hrde-1 (tm1200)*	*emb-4 (qm31)*
OFF (20/20)	ON (20/20)	ON (20/20)

Wild type	*hrde-1 (tm1200)*	*emb-4 (qm31)*
OFF (20/20)	ON (20/20)	ON (20/20)

Figure S4

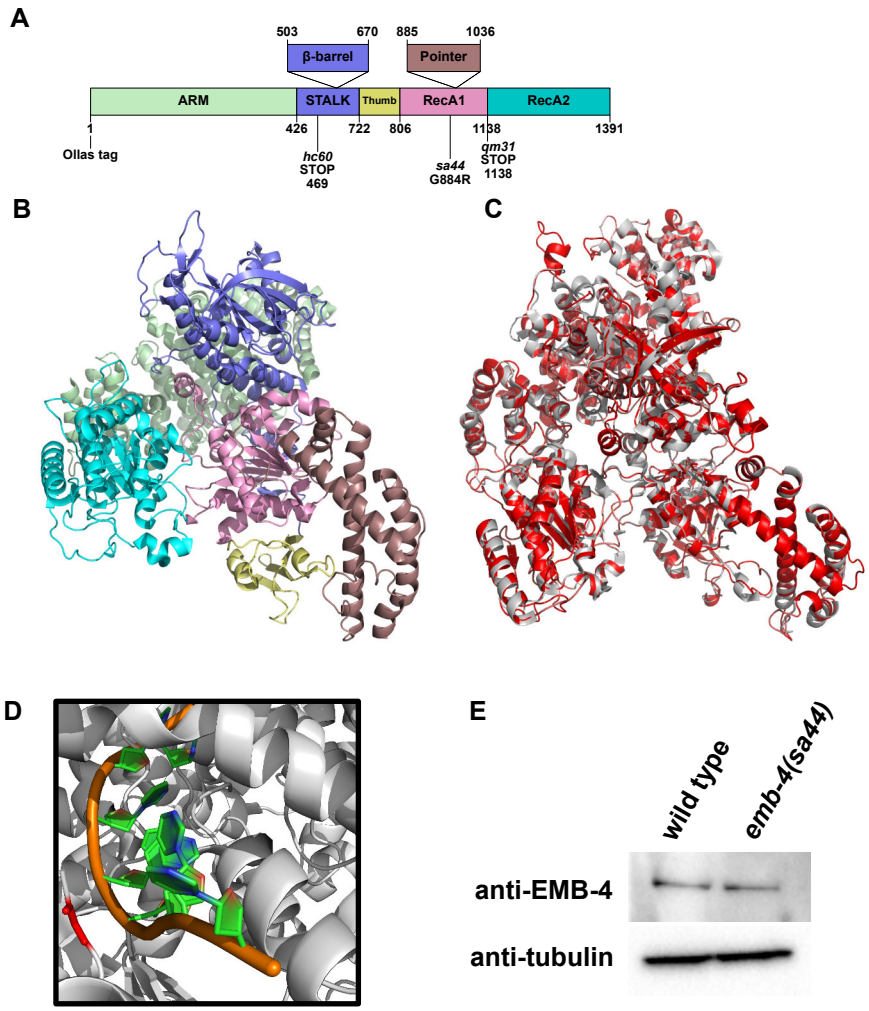
A
503
670
885
1036
β-barrel
Pointer
ARM
STALK
Thumb
RecA1
RecA2
1
426
722
806
1138
1391
Ollas tag
hc60
STOP
469
sa44
G884R
qm31
STOP
1138
B
C
D
E
wild type
emb-4(sa44)
anti-EMB-4
anti-tubulin

Figure S5

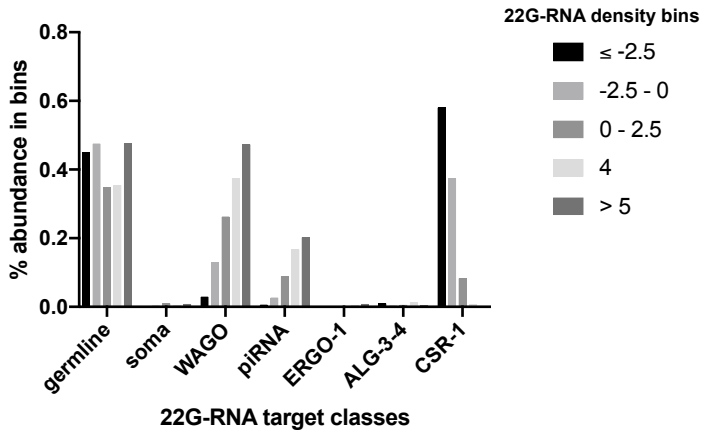
22G-RNA density bins
≤ -2.5
-2.5 - 0
0 - 2.5
4
> 5
% abundance in bins
0.8
0.6
0.4
0.2
0.0
germline
soma
WAGO
piRNA
ERGO-1
ALG-3-4
CSR-1
22G-RNA target classes

Figure S6

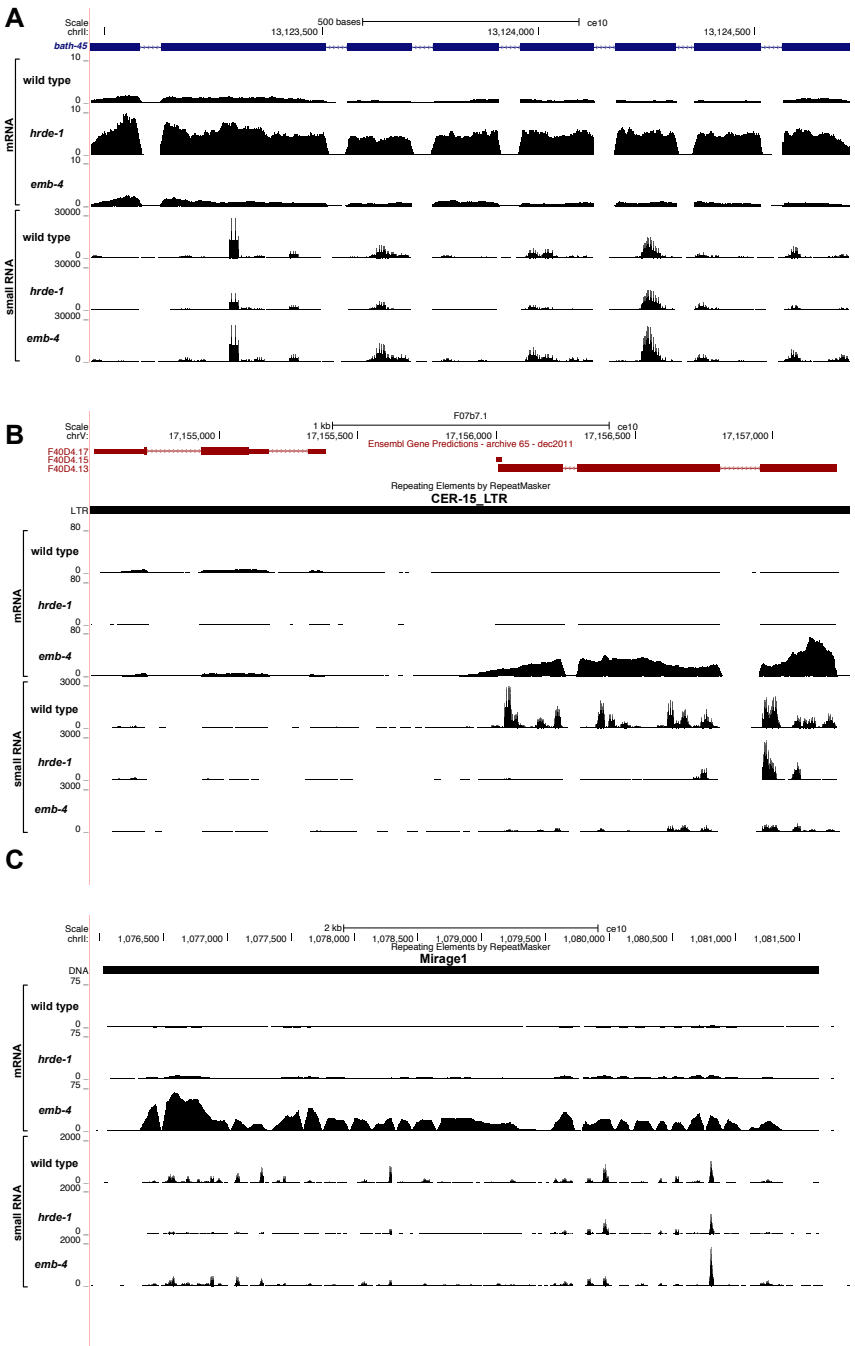
A
Scale
chrII:
500 bases
ce10
13,123,500
13,124,000
13,124,500
bath-45
mRNA
wild type
hrde-1
emb-4
small RNA
wild type
hrde-1
emb-4
B
Scale
chrV:
1 kb
F07b7.1
ce10
17,155,000
17,155,500
17,156,000
17,156,500
17,157,000
F40D4.17
F40D4.15
F40D4.13
Ensembl Gene Predictions - archive 65 - dec2011
Repeating Elements by RepeatMasker
CER-15_LTR
LTR
mRNA
wild type
hrde-1
emb-4
small RNA
wild type
hrde-1
emb-4
C
Scale
chrII:
2 kb
ce10
1,076,500
1,077,000
1,077,500
1,078,000
1,078,500
1,079,000
1,079,500
1,080,000
1,080,500
1,081,000
1,081,500
Repeating Elements by RepeatMasker
Mirage1
DNA
mRNA
wild type
hrde-1
emb-4
small RNA
wild type
hrde-1
emb-4

Figure S7

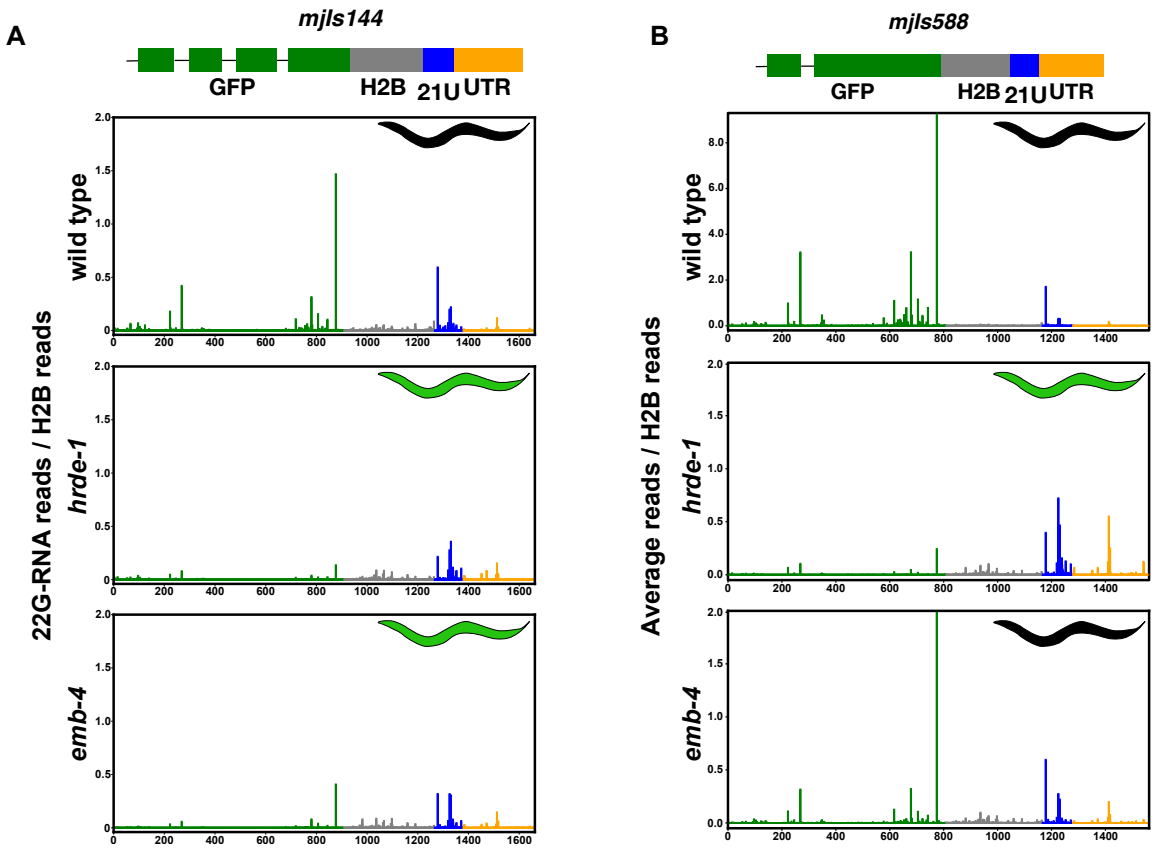
A
mjls144
GFP
H2B
21U
UTR
22G-RNA reads / H2B reads
wild type
hrde-1
emb-4
B
mjls588
Average reads / H2B reads

Figure S8

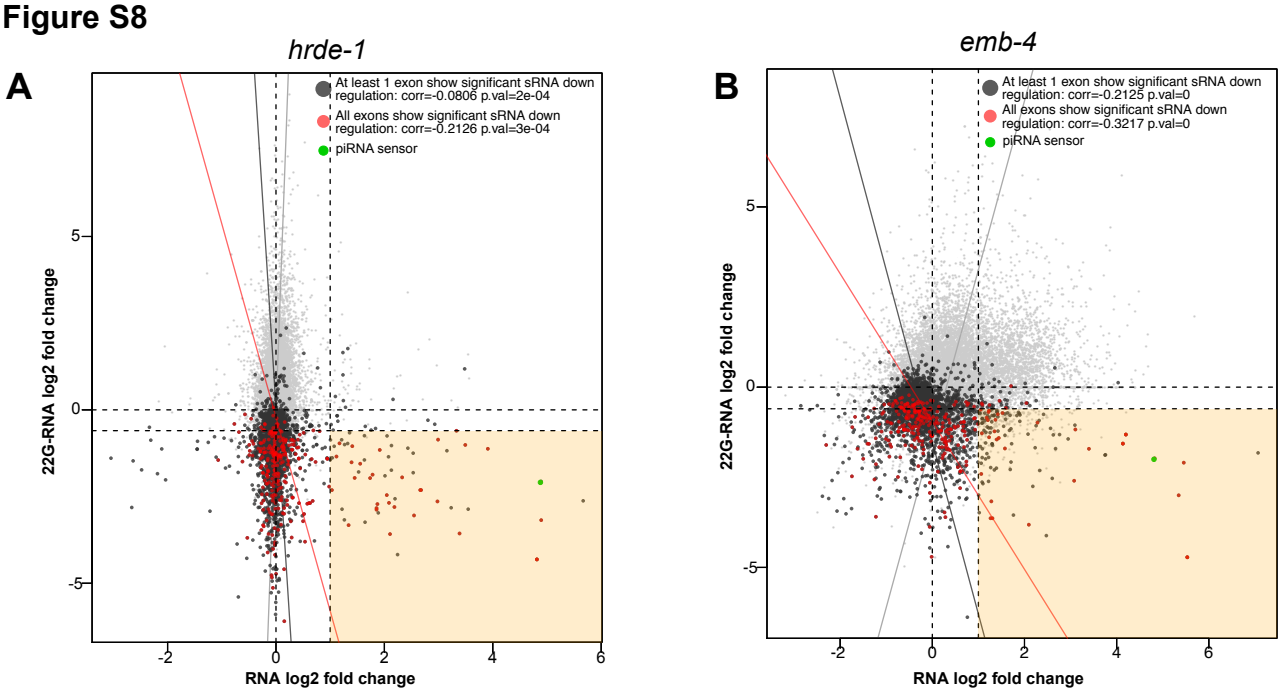
A
hrde-1
At least 1 exon show significant sRNA down regulation: corr=-0.0806 p.val=2e-04
All exons show significant sRNA down regulation: corr=-0.2126 p.val=3e-04
piRNA sensor
22G-RNA log2 fold change
RNA log2 fold change
B
emb-4
At least 1 exon show significant sRNA down regulation: corr=-0.2125 p.val=0
All exons show significant sRNA down regulation: corr=-0.3217 p.val=0
piRNA sensor
22G-RNA log2 fold change
RNA log2 fold change

Table S1

Table S1. Comparison of HRDE-1 interactors with PIWI interactors			
	***C. elegans* HRDE-1 IP mean log2 fold enrichment (# of replicates detected)**	***D. melanogaster* PIWI IP (Le Thomas et al., 2013)**	***D. melanogaster* PIWI IP (Le Thomas et al., 2013)**
ALYREF (ALY-3, ALY)	0.68 (2/3)	3/3	4/4
RPL23 (RPL-23, RpL23)	0.43 (3/3)	3/3	1/4
DDX4 (GLH-2, VAS)	0.57 (2/3)	2/3	4/4
RPS15 (RPS-15, RpS15)	0.36 (3/3)	2/3	2/4
EIF4A3 (MEL-46, eIF4AIII)	0.74 (3/3)	2/3	2/4
AQR (EMB-4, CG31368)	0.73 (2/3)	2/3	1/4
NCL (K07H8.10, CG17108)	0.70 (3/3)	2/3	-
SND1 (TSN-1, Tudor-SN)	0.36 (3/3)	1/3	-
POLR2C (RPB-3, RpII33)	0.64 (2/3)	-	3/4
RPL34 (RPL-34, RpL34)	0.39 (2/3)	-	2/4
NOP2 (NOL-1, CG8545)	0.63 (2/3)	-	2/4
SRRT (E01A2.2, ARS2)	0.40 (2/3)	-	2/4
POLR2J (RPB-11, Rpb11)	0.54 (2/3)	-	2/4
POLR1D (F58A4.9, l(2)37Cg)	0.64 (2/3)	-	2/4
SSB (C44E4.4, La)	0.61 (2/3)	-	2/4
NUP210 (NPP-12, Gp210)	0.60 (2/3)	-	-
IMP3 (C48B6.2, CG4866)	0.27 (3/3)	-	-
RPS13 (RPS-13, RpS13)	0.42 (3/3)	-	-
RRS1 (RRBS-1, CG32409)	0.50 (2/3)	-	-
DDX24 (F55F8.2, CG9143)	0.54 (2/3)	-	-
KIAA0020 (PUF-12, PEN)	0.50 (2/3)	-	-
DDX54 (Y94H6A.5, CG32344)	0.55 (2/3)	-	-
PAPD5 (GLD-4, TRF4)	0.88 (2/3)	-	-
HNRNPU (Y71G10AL.1, CG30122)	0.29 (3/3)	-	-
HNRNPR (HRP-2, SYP)	0.59 (3/3)	-	-
NUP93 (NPP-13, Nup93)	0.46 (3/3)	-	-
CSTF2 (R09B3.2, CstF-64)	0.36 (2/3)	-	-
POLR2B (RPB-2, RpII140)	0.63 (2/3)	-	-

Table S2

Table S2. Strains used in this study, related experimental procedures		
Strain	**Genotype**	**Comment**
SX1316	*mjIs144 II*	piRNA sensor transgene
SX2000	*mjIs144 II; hrde-1*(tm1200) III	
SX2929	*mjIs144* II*; emb-4*(qm31) V	
SX2930	*mjIs144* II; *emb-4*(hc60) V	
SX3041	*mjIs144* II; *emb-4*(sa44) V	
SX3073	*mjIs588* II	piRNA sensor with 1 intron
SX3074	*mjIs144* II; *hrde-1*(tm1200) III; *emb-4*(sa44) V	
SX3078	*mjIs588 II; hrde-1(tm1200) III*	
SX3079	*mjIs588 II; emb-4(qm31) V*	
VM285	*neSi21*	3XFLAG::HRDE-1
SX3117	*emb-4(mjSi92)*	Ollas::EMB-4